Available online at www.sciencedirect.com
SCIENCE DIRECT
Polymer 47 (2006) 4400–4410
polymer
www.elsevier.com/locate/polymer

Dispersion characteristics and rheology of organoclay nanocomposites based on a segmented main-chain liquid-crystalline polymer having side-chain azopyridine with flexible spacer

Wenyi Huang, Chang Dae Han *

Department of Polymer Engineering, The University of Akron, 250 South Forge Street, Akron, OH 44325, USA

Received 29 January 2006; received in revised form 14 April 2006; accepted 18 April 2006

Abstract

The dispersion characteristics and rheology of organoclay nanocomposites based on a main-chain liquid-crystalline polymer having side-chain azopyridine with flexible spacer (PABP) were investigated using X-ray diffraction (XRD), transmission electron microscopy (TEM), and oscillatory shear rheometry. In the preparation of nanocomposites via solution blending under vigorous stirring, two commercial organoclays (Southern Clay Products) were employed: one (Cloisite 30B) treated with a surfactant (MT2EtOH) having hydroxyl groups, and the other (Cloisite 20A) treated with a nonpolar surfactant (2M2HT) having hydrogenated tallow. Also prepared, for comparison, were nanocomposites prepared by mixing PABP with natural clay (montmorillonite, MMT). The following observations were made. (i) PABP/Cloisite 30B nanocomposite has featureless XRD patterns and a very high degree of dispersion of Cloisite 30B aggregates as determined from TEM. (ii) PABP/Cloisite 20A nanocomposite has shown a conspicuous XRD reflection peak and intercalation of Cloisite 20A aggregates as determined from TEM. (iii) PABP/MMT nanocomposite has shown XRD patterns, which are virtually the same as the XRD patterns of neat PABP with a slightly increased gallery distance, and it has very poor dispersion of MMT aggregates in the matrix of PABP. The observed high degree of dispersion of Cloisite 30B aggregates in PABP/Cloisite 30B nanocomposite is attributable to the formation of hydrogen bonds between the pyridyl group of side-chain azopyridine and the hydroxyl groups in the surfactant MT2EtOH residing at the surface of Cloisite 30B. The presence of hydrogen bonds in the PABP/Cloisite 30B nanocomposite was confirmed by in situ Fourier transform infrared (FTIR) spectroscopy. It was observed via polarized optical microscopy that the liquid crystallinity of PABP in the PABP/Cloisite 30B nanocomposites was more or less intact with a very high degree of dispersion of Cloisite 30B aggregates. Oscillatory shear flow measurements of the organoclay nanocomposites prepared support the conclusions drawn from XRD, TEM, and FTIR spectroscopy.

Keywords: Liquid-crystalline polymers; Organoclay; Nanocomposites

1. Introduction

During the last decade, well over 1000 articles [1] have been reported in the literature dealing with the preparation of organoclay nanocomposites. The primary goal in preparing organoclay nanocomposites is to achieve a very high degree of dispersion (commonly referred to as exfoliation) of organoclay aggregates that will generate very large surface areas, which then would, hopefully, significantly improve the mechanical properties of the nanocomposites. However, the realization of significant improvement in the mechanical properties of organoclay nanocomposites has not materialized to a large extent. The majority of the studies reported on organoclay nanocomposites have shown intercalation of organoclay aggregates in the polymer matrix. Such an experimental observation is attributed to the lack of compatibility between the polymer matrix and organoclay employed. In other words, in the absence of strong attractive interactions between organoclay and polymer matrix, little can be expected in the way of achieving a very high degree of dispersion of organoclay aggregates by the polymer matrix. This means that a judicious choice of organoclay and polymer matrix must be made to achieve a very high degree of dispersion of organoclay aggregates. For such purposes, one must design and synthesize a polymer that can have strong attractive interactions with the selected organoclay and/or develop a

* Corresponding author. Tel.: +1 330 972 6468; fax: +1 330 972 5720.
E-mail address: cdhan@uakron.edu (C.D. Han).

0032-3861/$ - see front matter © 2006 Elsevier Ltd. All rights reserved.
doi:10.1016/j.polymer.2006.04.034

surfactant(s) that can be used to treat natural clay or layered silicates, such that the chemically modified clay can have strong attractive interactions with the selected polymer.

In the past, numerous attempts have been made to prepare organoclay nanocomposites having a high degree of dispersion using many different commercial thermoplastic polymers, such as polypropylene [2–6], polyamides [7–12], polystyrene [13–15], poly(ethylene oxide) [16,17,26], poly(L-lactide) [18], poly(vinyl pyridine) [19], poly(ε-caprolactone) [20–24], polycarbonate [25], poly(ethylene-*ran*-vinyl acetate) [26–29], and poly(ethylene-*ran*-vinyl acetate-*ran*-vinyl alcohol) [30]. The references cited above are by no means exhaustive. The majority of the studies cited above failed to obtain a very high degree of dispersion of organoclay aggregates, primarily because there was a lack of sufficient compatibility between the polymer matrix and the organoclay employed. The readers are referred to a few review articles [31–34] that describe some fundamental aspects of the preparation of organoclay nanocomposites based on thermoplastic polymers.

However, only a few studies [35,36] have been reported on the preparation of organoclay nanocomposites based on thermotropic liquid-crystalline polymer (TLCP). And, these studies only showed intercalation of organoclay aggregates in the nanocomposites prepared. This is not surprising, because no compatibility (i.e. no attractive interactions) existed between the organoclays and TLCPs employed. There are only a few commercial TLCPs available (e.g. copolyesters of *p*-hydroxybenzoic acid (HBA) and poly(ethylene terephthalate) (PET); copolyesters of HBA and 6-hydroxy-2-naththoic acid (HNA)). In the absence of functionality in those commercial TLCPs, the prospects for achieving a very high degree of dispersion of organoclay aggregates are very low. Further, chemical modification of the commercial TLCPs would be extremely difficult, if not impossible, to incorporate functionality. This then suggests that a new generation of TLCPs must be synthesized for such purposes.

In a previous study [37], we synthesized a segmented main-chain TLCP having pendent pyridyl group (referred to as PyHQ12), the chemical structure of which is given below. PyHQ12 was then used to prepare organoclay nanocomposites. We found that PyHQ12 was very effective to achieve a very high degree of dispersion of the organoclay aggregates having hydroxyl groups. Using Fourier transform infrared (FTIR) spectroscopy we have confirmed the formation of hydrogen bonds between the pendent pyridyl group in PyHQ12 and the hydroxyl group in the surfactant residing at the surface of the organoclay. But, a significant degree of liquid crystallinity of PyHQ12 in the organoclay nanocomposite was lost due to the formation of hydrogen bonds. We then realized that this was due to the proximity of the pendent pyridyl group to the mesogenic main-chain backbone. In other words, the pendent pyridyl group was located so close to the mesogenic main-chain backbone of PyHQ12, that hydrogen bonding between the pendent pyridyl group in PyHQ12 and the hydroxyl group in the surfactant residing at the surface of organoclay greatly restricted the mobility (thus orientation) of the mesogenic main chain of PyHQ12.

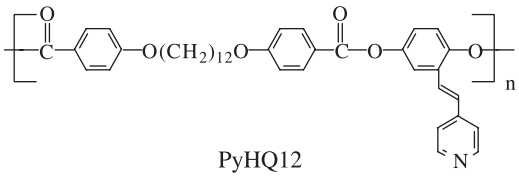

PyHQ12

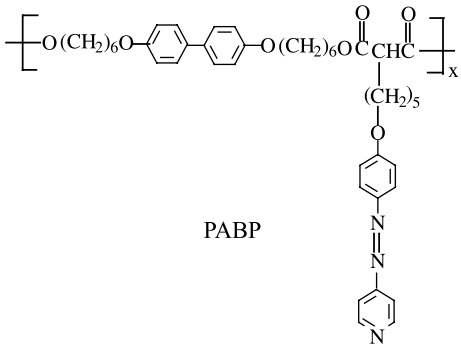

PABP

To overcome the undesirable feature described above, subsequently we synthesized a new segmented main-chain TLCP (referred to as PABP) having side-chain azopyridyine with flexible spacer, the chemical structure of which is shown below

In this study, we have found that the liquid crystallinity of PABP in the organoclay nanocomposites was more or less intact and yet organoclay aggregates were very well dispersed. Thus, our goal to obtain a highly dispersed organoclay nanocomposite based on a segmented main-chain TLCP has been accomplished. In this paper, we summarize the highlights of our findings.

2. Experimental

2.1. Materials and preparation of nancomposites

The details of the synthesis procedures, thermal transitions, and also the mesophase structure of the liquid-crystalline polymer PABP employed in the present study are described elsewhere [38]. Note that the chemical structure of PABP is given above.

In the present study, we employed two commercial organoclays supplied by Southern Clay Products. They are: (i) Cloisite 30B treated with a surfactant (MT2EtOH) having the chemical structure methylbis-2-hydroxyethyltallow alkyl quaternary ammonium chloride, and (ii) Cloisite 20A treated with a surfactant (2M2HT) having the chemical structure dimethyldihydrogenated tallow alkyl quaternary ammonium chloride. The chemical structures of the surfactants, MT2EtOH and 2M2HT, are given below [39].

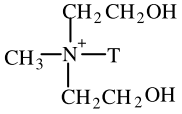

MT2EtOH

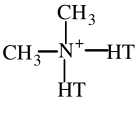

2M2HT

In the chemical structure of MT2EtOH, N^+ denotes quaternary ammonium chloride and T denotes tallow consisting of ca. 65% C18, ca. 30% C16, and ca. 5% C14, and in the chemical structure of 2M2HT, N^+ denotes quaternary ammonium chloride and HT denotes hydrogenated tallow consisting of ca. 65% C18, ca. 30% C16, and ca. 5% C14. Note that 100% of Na^+ ions in natural clay (montmorillonite, MMT) have been exchanged [39]. According to the Technical Properties Bulletin [39] from Southern Clay Products, the amount of surfactant MT2EtOH residing at the surface of Cloisite 30B is 90 mequiv./100 g and the amount of surfactant 2M2HT residing at the surface of Cloisite 20A is 95 mequiv./100 g. Using methanol, we washed the organoclays, before use, to remove any excess surfactant. Note that Cloisite 30B has hydroxyl groups while Cloisite 20A does not, as confirmed by Fourier transform infrared (FTIR) spectroscopy [30]. The reason for having chosen these two organoclays lies in that we were interested in demonstrating that compatibility, via specific interactions, between PABP and an organoclay is necessary to achieve a very high degree of dispersion of organoclay aggregates.

We prepared organoclay nanocomposites by solution blending; namely, a predetermined amount of PABP was dissolved in pyridine upon heating to 80 °C and then an organoclay suspended in pyridine was added slowly, while vigorously stirring, into the polymer solution. The solvent in the mixture was evaporated slowly under constant stirring for 2 days. The mixture of PABP with an organoclay was dried completely in a vacuum oven at temperatures well above the boiling point of pyridine and also at ca. 20 °C above the melting temperature (T_m) of PABP until no weight changes were detected. The amount of organoclay used was 5 wt% in all nanocomposites. Since, the amount of surfactant MT2EtOH (or 2M2HT) residing at the surface of Cloisite 30B (or Cloisite 20A) is 32 wt%, the net amount of clay was 3.4 wt% in each nanocomposite.

2.2. X-ray diffraction (XRD)

Wide-angle X-ray scattering was conducted at ambient temperature on a Rigaku Rotaflex rotating anode diffractometer with slit collimation. The X-ray generator was operated at 40 kV and 150 mA, and the X-ray beam was monochromatized to CuK_α with a graphite crystal. The range of 2θ scanning of X-ray intensity employed was 1.5–10°. X-ray diffraction (XRD) patterns were obtained to determine the mean interlayer spacing of the (001) plane (d spacing) for the organoclay (Cloisite 20A or Cloisite 30B) and its nanocomposites with PABP.

2.3. Wide-angle X-ray diffraction (WAXD)

WAXD experiments were conducted at room temperature on the as-cast films of neat PABP using a general electric X-ray generator (Model XRD-6) operated at 30 kV and 30 mA (Ni-filtered CuK_α radiation). The flat-plate diffraction patterns were recorded with a 53.3 mm film-to-specimen distance. The exposure time for each measurement was 4 h.

2.4. Transmission electron microscopy (TEM)

TEM images of specimens were taken at room temperature. The ultrathin sectioning (50–70 nm) of specimens was performed by ultramicrotomy cryogenically for the nanocomposites based on PABP. A transmission electron microscope (JEM1200EX 11, JEOL) operated at 120 kV was used to obtain images of the nanocomposite specimens.

2.5. Oscillatory shear rheometry

An advanced rheometric expansion system (ARES, TA Instruments) was used in the oscillatory mode with parallel plate fixtures (8 mm diameter). Dynamic temperature sweep experiments under isochronal conditions were conducted, i.e. the dynamic storage modulus (G') and dynamic loss modulus (G'') were measured at an angular frequency (ω) of 0.1 rad/s during heating, and the complex viscosity ($|\eta^*|$) was calculated using the expression, $|\eta^*(\omega)| = \{[G'(\omega)/\omega]^2 + [G''(\omega)/\omega]^2\}^{1/2}$. We also conducted dynamic frequency sweep experiments using a parallel plate fixture (8 mm diameter), measuring G' and G'' as functions of ω (ranging from 0.03 to 100 rad/s) at various temperatures between 120 and 160 °C, for which a fixed strain of 0.04 was used to ensure that measurements were taken well within the linear viscoelastic range of the materials investigated. Data acquisition was accomplished with the aid of a microcomputer interfaced with the rheometer. The temperature control was satisfactory to within ± 1 °C. All experiments were conducted under a nitrogen atmosphere to preclude oxidative degradation of the samples.

2.6. Fourier transform infrared (FTIR) spectroscopy

Using a Fourier transform infrared spectrometer (16 PC FTIR, Perkin–Elmer), in situ FTIR spectra were obtained at temperatures ranging from 25 to 160 °C for PABP/Cloisite 30B nanocomposites. The temperature was measured at the sample surface and controlled to within ± 1.0 °C using a proportional-integral-derivative controller. Specimens were maintained at a preset temperature for 5 min prior to data acquisition. FTIR spectra for other specimens were obtained at room temperature. Spectral resolution was maintained at 4 cm^{-1}. Dry nitrogen gas was used to purge the sample compartment to reduce the interference of water and carbon dioxide in the spectrum. Thin films suitable for FTIR spectroscopy were prepared by casting 2% (w/v) solution in pyridine directly on the KBr salt plate. Film thickness was adjusted, such that the maximum absorbance of any band was less than 1.0, at which the Beer–Lambert law is valid. Film specimens were slowly dried for 24 h in a fume hood until most of the solvent evaporated and then dried at 100 °C for a few days in a vacuum oven, and they were then stored in a vacuum oven until use.

2.7. Polarized optical microscopy (POM)

The mesophase structures of the liquid-crystalline phase of PABP and its nanocomposites were investigated, via POM, using a Leitz Laborlux 12 Pol S polarized optical microscope

equipped with a hot stage (Instec) and a digital camera (Spot insight 2, Diagnostic Instrument Inc.). Specimens were cast from 1 wt% solution of neat PABP or its nanocomposites on a slide glass to obtain a film of about 2–3 μm in thickness, which was then first dried in a fume hood and then in a vacuum oven. The heating and cooling rates employed were 3 °C/min. Images of POM were obtained after keeping a specimen at a preset temperature for at least 10 min.

2.8. Differential scanning calorimetry (DSC)

The phase transition temperatures of PABT and its nanocomposites were determined, via differential scanning calorimetry (Perkin-Elmer DSC-7 series), using indium as the calibration standard at a heating rate of 20 °C/min under a nitrogen atmosphere.

3. Results and discussion

3.1. Thermal transition temperatures and mesophase structure of organoclay nanocomposites based on PABP

Fig. 1 gives the DSC thermograms at a heating rate of 20 °C/min for (a) neat PABP, (b) PABP/MMT nanocomposite, (c) PABP/Cloisite 20A nanocomposite, and (d) PABP/Cloisite 30B nanocomposite. The following observations are worth noting in Fig. 1. (i) Neat PABP is a semicrystalline TLCP having a melting temperature (T_m) of ca. 114 °C (the lower endothermic peak) and a clearing (isotropization) temperature (T_{cl}) of ca. 146 °C (the upper endothermic peak). (ii) The DSC thermogram for PABP/MMT nanocomposite is virtually identical to that for neat PABP, suggesting that the presence of MMT has not affected the thermal transition temperatures of PABP and thus, no attractive interaction exists between MMT and PABP. (iii) The DSC thermogram for PABP/Cloisite 20A nanocomposite shows that both T_m and T_{cl} are increased only by ca. 0.5 °C over those of neat PABP, the increase being practically insignificant.

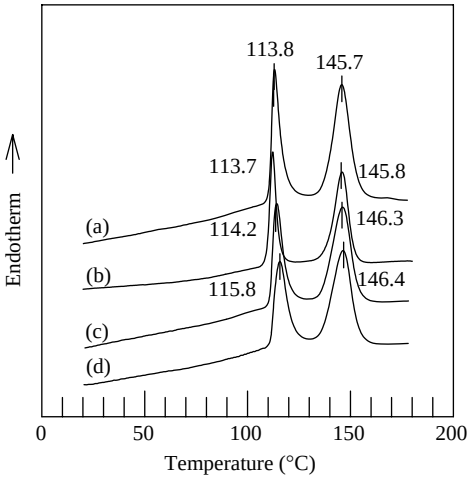

Fig. 1. DSC thermograms for (a) PABP, (b) PABP/MMT nanocomposite, (c) PABP/Cloisite 20A nanocomposite, and (d) PABP/Cloisite 30B nanocomposite at a heating rate of 20 °C/min during the heating cycle.

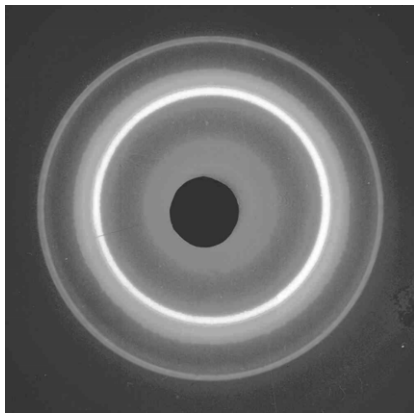

Fig. 2. WAXD powder patterns of PABP.

(iv) The DSC thermogram for PABP/Cloisite 30B nanocomposite shows that T_m is increased by ca. 2 °C and T_{cl} is increased only by ca. 0.7 °C. In view of the fact that the T_{cl} of PABP in the PABP/Cloisite 20A and PABP/Cloisite 30B nanocomposites increased only slightly (0.5–0.7 °C) over that of neat PABP, we can tentatively conclude that the mesophase structure of PABP in both nanocomposites might be very little different from that of neat PABP. It is worth noting in Fig. 1 that the area under the upper endothermic peak is virtually identical for all three nanocomposites, suggesting further that the mesophase structure of neat PABP might have changed very little.

Having concluded from the DSC thermograms given in Fig. 1 that PABP is a semicrystalline TLCP, we conducted WAXD experiments to characterize the mesophase structure of PABP. Fig. 2 gives WAXD powder patterns for a PABP specimen, which was taken at room temperature. It is seen from Fig. 2 that the WAXD powder patterns have a sharp inner reflection and a diffuse outer halo, indicative of the presence of a smectic mesophase [40,41]. From this observation we conclude that at temperatures between ca. 114 and ca. 146 °C PABP has only a smectic mesophase and thus the upper endothermic peak in the

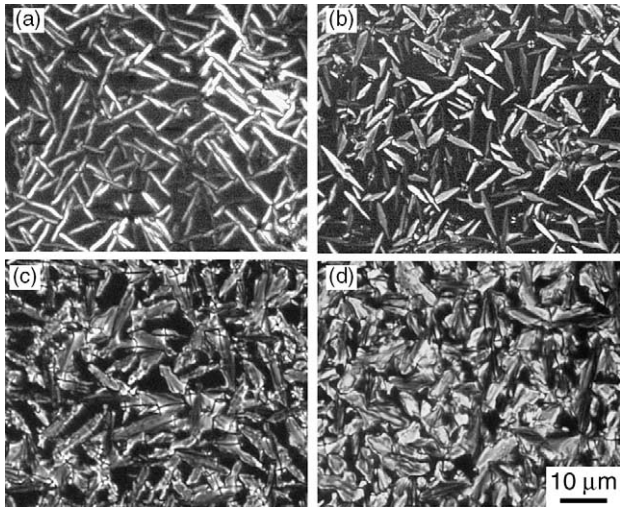

Fig. 3. POM images for (a) PABP, (b) PABP/MMT nanocomposites (c) PABP/Cloisite 20A nanocomposites, and (d) PABP/Cloisite 30B nanocomposites.

DSC thermogram given in Fig. 1 represents a smectic-to-isotropic (S–I) transition temperature (T_{SI}).

Fig. 3 gives POM images of (a) PABP, (b) PABP/MMT nanocomposite, (c) PABP/Cloisite 20A nanocomposite, and (d) PABP/Cloisite 30B nanocomposite. Notice in Fig. 3 that PABP has a smectic phase, and the mesophase structure of PABP/MMT nanocomposite is virtually identical to that of PABP, while the mesophase structure of PABP in the PABP/Cloisite 20A and PABP/Cloisite 30B nanocomposites is only slightly different from that of neat PABP. This observation is consistent with that made above from the DSC thermograms given in Fig. 1. Thus, we can conclude that the presence of organoclay in both PABP/Cloisite 20A and PABP/Cloisite 30B nanocomposites has affected little the mesophase structure of PABP in the respective nanocomposites. What remains to be seen is whether the degree of dispersion of organoclay aggregates in the respective nanocomposites might be the same or not.

3.2. Dispersion characteristics of organoclay nanocomposites based on PABP

3.2.1. X-ray diffraction (XRD) patterns of organoclay nanocomposites based on PABP

Fig. 4(a) gives XRD patterns for MMT having a gallery distance (d_{001} spacing) of 1.1 nm, Cloisite 30B having a d spacing of 1.9 nm, and Cloisite 20A having a d spacing of 3.1 nm. It is seen that chemical treatment of MMT with a surfactant has increased the gallery distance of the respective organoclays. Fig. 4(b) gives XRD patterns for (1) neat PABP, (2) PABP/MMT nanocomposite, (3) PABP/Cloisite 30B nanocomposite, and (4) PABP/Cloisite 20A nanocomposite. Since, PABP is a semicrystalline TLCP as evidenced by the DSC thermogram given in Fig. 1 and by the WAXD powder patterns given in Fig. 2, the two XRD peaks at 2θ of ca. 3.75 and 7.40° observed in Fig. 4(b) are attributable to the smectic layered mesophase structure of PABP, as evidenced by the variation in the X-ray diffraction intensity during the second heating cycle [38]. Notice in Fig. 4(b) that the XRD peak at $2\theta = 7.40°$ appears in all three nanocomposites and the XRD peak at $2\theta = 3.75°$ also appears in the PABP/MMT nanocomposite. This observation suggests that the mesophase structure of PABP in the PABP/MMT nanocomposite might have been little affected although the d spacing of MMT has increased by 0.5 nm. Indeed, from the POM image given in Fig. 3(b) we already have observed little change in the mesophase structure of PABP in the PABP/MMT nanocomposite.

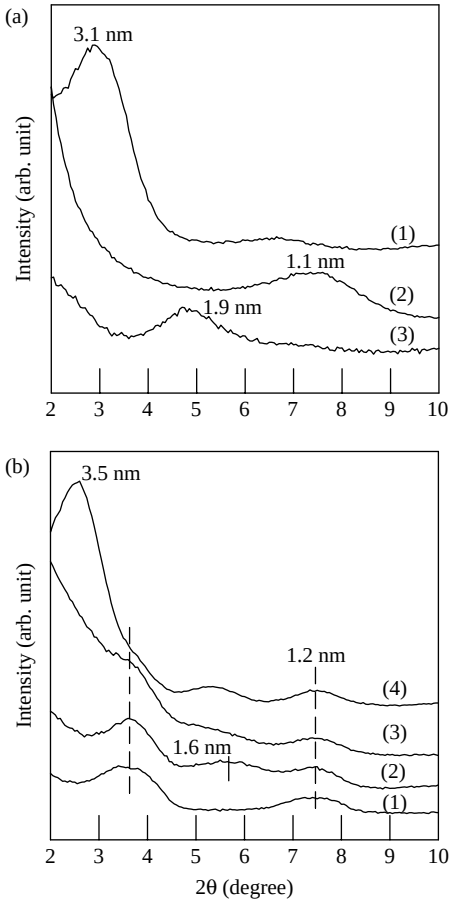

Fig. 4. XRD patterns for: (a) (1) Cloisite 20A, (2) MMT, and (3) Cloisite 30B; (b) (1) PABP, (2) PABP/MMT nanocomposite, (3) PABP/Cloisite 20A nanocomposite, and (4) PABP/Cloisite 30B nanocomposite.

However, the XRD peak at $2\theta = 3.75°$ due to the mesophase structure of PABP is not very discernible in Fig. 4(b) for the PABP/Cloisite 20A and PABP/Cloisite 30B nanocomposites. This observation suggests that some type of interaction between the organoclay and PABP might have occurred, supporting the slight change in the mesophase structure of PABP observed in the respective nanocomposites (see the POM images given in Fig. 3(c) and (d)). Notice in Fig. 4 that the d spacing of Cloisite 20A in PABP/Cloisite 20A nanocomposite has increased only slightly from 3.1 to 3.5 nm, but interestingly the PABP/Cloisite 30B nanocomposite shows virtually featureless XRD patterns. This observation seems to suggest the presence of strong attractive interactions between PABP and Cloisite 30B in the PABP/Cloisite 30B nanocomposite. We hasten to point out that the disappearance of the XRD peak does not necessarily signify that organoclay aggregates are highly dispersed.

3.2.2. Transmission electron microscopy (TEM) of organoclay nanocomposites based on PABP

Fig. 5 gives TEM images of PABP/MMT, PABP/Cloisite 20A, and PABP/Cloisite 30B nanocomposites. In Fig. 5 we observe (i) very poor dispersion of MMT aggregates in PABP/MMT nanocomposite, (ii) intercalation of Cloisite 20A aggregates in PABP/Cloisite 20A nanocomposite, and (iii) very high degree of dispersion of Cloisite 30B aggregates in PABP/Cloisite 30B nanocomposite. These observations are consistent with those made above from the XRD patterns given in Fig. 4(b). What is significant here is that a very high degree of dispersion of Cloisite 30B aggregates has affected little the mesophase structure (liquid crystallinity) of PABP in the PABP/Cloisite 30B nanocomposite (Fig. 3). This was not the case for the PyHQ12/Cloisite 30B nanocomposite described in our previous paper [37], in which much of the liquid crystallinity of a segmented main-chain TLCP, PyHQ12,

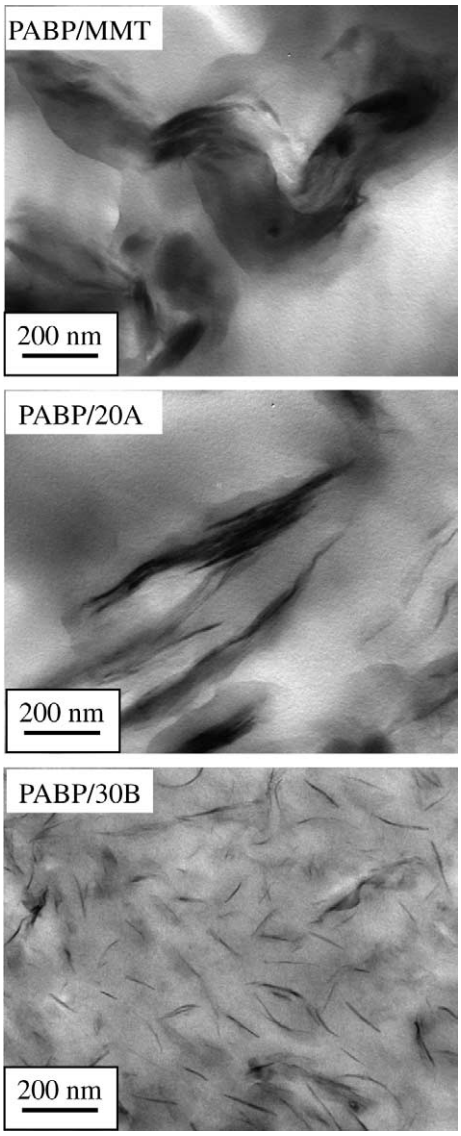

Fig. 5. TEM images of PABP/Cloisite 30B nanocomposite, PABP/Cloisite 20A nanocomposite, and PABP/MMT nanocomposite, in which the dark areas represent the clay and the gray/white areas represent the polymer matrix.

was lost while Cloisite 30B aggregates were dispersed very well in the matrix of PyHQ12. The origin of the difference between the two situations, PABP/Cloisite 30B nanocomposite and PyHQ12/Cloisite 30B nanocomposite, will be elaborated on later in this paper.

3.2.3. Fourier transform infrared (FTIR) spectroscopy of organoclay nanocomposites based on PABP

Fig. 6 gives FTIR spectra for (a) neat PABP at room temperature, (b) PABP/MMT nanocomposite at room temperature, (c) PABP/Cloisite 20A nanocomposite at room temperature, and (d) in situ FTIR spectra for PABP/Cloisite 30B nanocomposite at various temperatures ranging from 25 to 160 °C. It can be seen in Fig. 6 that neat PABP has two absorption peaks (spectrum a), a broad peak at a wavenumber of 2560 cm^{-1} and another at a wavenumber of 1890 cm^{-1}. These two absorption peaks indicate the presence of attractive

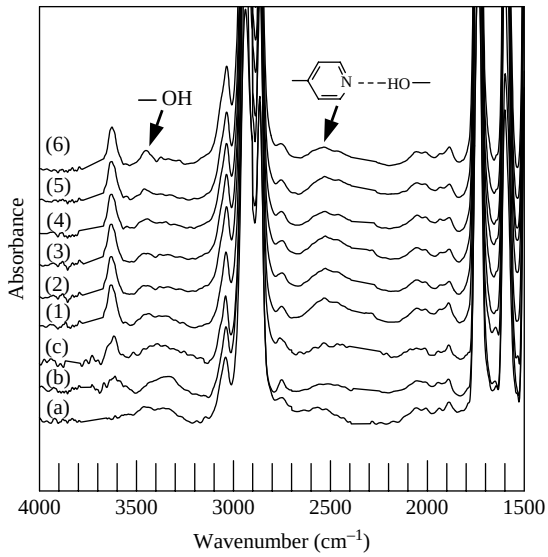

Fig. 6. FTIR spectra for: (a) PABP, (b) PABP/MMT nanocomposite, (c) PABP/Cloisite 20A nanocomposite, and in situ FTIR spectra for PABP/Cloisite 30B nanocomposite at various temperatures (°C): (1) 25, (2) 100, (3) 120, (4) 140, (5) 150, and (6) 160.

interactions, though very weak, between the pyridyl group in the side-chain azopyridine and hydroxyl groups at the end of the main chain of PABP (see the chemical structure of PABP given above). It should be mentioned that after polymerization is completed, 50% of the terminal groups in PABP macromolecular chains could be hydroxyl groups. Thus, the absorption peak at a wavenumber of 2560 cm^{-1} is believed to represent hydrogen bonds formed between the terminal hydroxyl group at the end of the main chain of PABP and the pyridyl group in the side-chain azopyridine (i.e. self-association in PABP), while the absorption peak at a wavenumber of 1890 cm^{-1} represents Fermi resonance.

Referring to Fig. 6, little evidence can be seen of the presence of hydrogen bonds in the PABP/MMT nanocomposite (spectrum b) and a very weak interaction in PABP/Cloisite 20A nanocomposite (spectrum c), while the in situ spectra (1–6) for PABP/Cloisite 30B nanocomposite indicate the presence of strong attractive interactions. Notice in Fig. 6 that the size (or area) of the absorption peak at 2570 cm^{-1} for the PABP/Cloisite 30B nanocomposite is larger than that for neat PABP although it tends to decrease, while the size of the absorption peak at 3460 cm^{-1} for the hydroxyl group tends to increase, as the temperature is increased to 160 °C. Of particular note in the FTIR spectra for the PABP/Cloisite 30B nanocomposite displayed in Fig. 6 is that the relatively strong absorption peak at 2570 cm^{-1} persists even at a temperature as high as 160 °C, which is above the clearing temperature of PABP (Fig. 1). This observation will be important later to explain the rheological behavior of PABP/Cloisite 30B nanocomposite. Thus, we conclude that attractive interactions exist (i.e. hydrogen bonds are formed) between the pyridyl group in the side-chain azopyridine and the hydroxyl group in the surfactant MT2EtOH residing at the surface of organoclay

Cloisite 30B. We conclude further that the presence of hydrogen bonding in the PABP/Cloisite 30B nanocomposite helped achieve a very high degree of dispersion of Cloisite 30B aggregates in the PABP matrix (see the TEM image given in Fig. 5). Earlier, Sato et al. [42] reported on hydrogen bonding between a polymer containing pyridine group and another polymer with hydroxyl group. Some investigators [43–45] reported on an improvement in miscibility between two polymers via hydrogen bonding.

The above observations can now explain the reasons for the very poor dispersion of MMT aggregates in PABP/MMT nanocomposite, some intercalation of Cloisite 20A aggregates in PABP/Cloisite 20A nanocomposite, and a very high degree of dispersion of Cloisite 30B aggregates in PABP/Cloisite 30B nanocomposite (Fig. 5).

3.3. Rheological behavior of organoclay nanocomposites based on PABP

Fig. 7 describes the frequency dependence of the dynamic storage modulus (G') for (a) PABP, (b) PABP/MMT nanocomposite, (c) PABP/Cloisite 20A nanocomposite, and (d) PABP/Cloisite 30B nanocomposite at various temperatures below and above the isotropization temperature of PABP as determined by the upper endothermic peak in the DSC thermograms (Fig. 1). Below we will refer to the isotropization temperature of each material as smectic-to-isotropic transition temperature (T_{SI}) since we have confirmed that all four materials have smectic mesophase at temperatures between the melting temperature (the lower endothermic peak in the DSC thermogram) and the isotropization temperature (the upper endothermic peak in the DSC thermogram). The following observations are worth noting in Fig. 7.

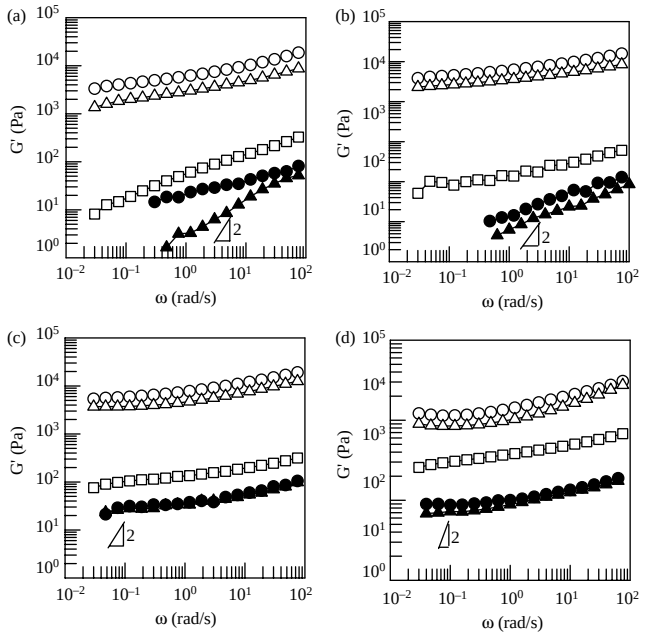

Fig. 7. Log G' versus log ω plots for (a) PABP, (b) PABP/MMT nanocomposite, (c) PABP/Cloisite 20A nanocomposite, and (d) PABP/Cloisite 30B nanocomposite at different temperatures (°C): (○) 120, (△) 130, (□) 140, (●) 150, and (▲) 160.

Referring to Fig. 7(a), in the isotropic state at 160 °C that is ca. 14 °C above the T_{SI} (ca. 146 °C) of PABP, the slope of log G' versus log ω plot in the terminal region for neat PABP is much less than two. Such unusual rheological characteristics have never been observed for typical TLCPs and flexible homopolymers. We attribute this observation to the self-association taking place within the PABP molecules having pyridyl groups in the side-chain azopridine as well as the hydroxyl group at the end of the main chain of PABP, as pointed out above in reference to the FTIR spectra given in Fig. 6. A similar observation can be made in Fig. 7(b) for the PABP/MMT nanocomposite, suggesting that the presence of MMT has not influenced the frequency dependence of PABP in the nanocomposite. This can be explained by the fact that there are little or no attractive interactions between MMT and PABP, as evidenced by XRD patterns (Fig. 4) and by TEM image (Fig. 5).

However, the situation becomes quite different for the PABP/Cloisite 20A nanocomposite given in Fig. 7(c) and for the PABP/Cloisite 30B nanocomposite given in Fig. 7(d). Namely, referring to Fig. 7(c), the slope of log G' versus log ω plot in the terminal region for the PABP/Cloisite 20A nanocomposite in the isotropic state is extremely small with a downward trend at angular frequencies below about 0.1 rad/s. Such rheological characteristics seem to indicate the presence of some interactions between the organoclay Cloisite 20A and PABP, different from the rheological characteristics observed in Fig. 7(b) for the PABP/MMT nanocomposite. Indeed we already have observed the presence of a weak interaction in the PABP/Cloisite 20A nanocomposite from the FTIR spectrum given in Fig. 6. However, although we observe a similar trend in Fig. 7(d) for the PABP/Cloisite 30B nanocomposite, there is a subtle difference between the PABP/Cloisite 30B and PABP/Cloisite 20A nanocomposites in that no downward trend in the terminal region of log G' versus log ω plot is discernible for the PABP/Cloisite 30B nanocomposite. Most importantly, values of G' in the terminal region of log G' versus log ω plot for the PABP/Cloisite 30B nanocomposite are an order of magnitude larger than those for the PABP/Cloisite 20A nanocomposite. Such a significant difference between the two nanocomposites is attributable to the presence of strong attractive interactions, via hydrogen bonding, between the pyridyl group in the side-chain azopyridine of PABP and the hydroxyl groups in the surfactant MT2EtOH residing at the surface of Cloisite 30B. What is remarkable here is the observation, which can be made from Fig. 7(d), that apparently the strength of hydrogen bonding in the isotropic state of PABP/Cloisite 30B nanocomposite is very high at 160 °C, which is above the T_{SI} (ca. 147 °C) of PABP in the nanocomposite. We hasten to point out that PABP begins to undergo thermal degradation at ca. 285 °C as determined from thermal gravimetric analysis. Thus, there is no chance whatsoever for thermal degradation/crosslinking to have caused the very unusual rheological behavior displayed in Fig. 7. It has generally been observed

that the strength of hydrogen bonding decreases with increasing temperature [46].

It is fair to state that the greater the strength of hydrogen bonding, the better the compatibility between the organoclay Cloisite 30B and the matrix PABP in the PABP/Cloisite 30B nanocomposite, giving rise to an improved dispersion of organoclay aggregates in the nanocomposite owing to the larger surface areas available. In turn, the larger the surface areas available, the greater will be the values of G' in the nanocomposites. This is precisely the reason why in Fig. 7(d) we observe such large values of G' in the terminal region of $\log G'$ versus $\log \omega$ plot for the PABP/Cloisite 30B nanocomposite, as compared to the PABP/MMT and PABP/Cloisite 20A nanocomposites. Referring to Fig. 7(d), it should be pointed out further that the solid-like rheological behavior at temperatures below the T_{SI} (ca. 147 °C) of PABP arises in large part from the mesophase structure (Fig. 3) of PABP. However, the solid-like rheological behavior of the PABP/Cloisite 30B nanocomposite at temperatures above the T_{SI} (ca. 147 °C) of PABP is solely due to the strong attractive interactions in the nanocomposites. Hence, we can conclude that the results of rheological measurements displayed in Fig. 7 shed an additional light on the mechanism that explains why the PABP/Cloisite 30B nanocomposite has a very high degree of dispersion of Cloisite 30B aggregates in the matrix PABP.

Fig. 8 describes the temperature dependence of G' during isochronal temperature sweep experiments at an angular frequency of 0.1 rad/s for PABP (○), PABP/MMT nanocomposite (△), PABP/Cloisite 20A nanocomposite (□), and PABP/Cloisite 30B nanocomposite (▽). In Fig. 8 we observe that values of G' for PABP initially decrease very slowly with increasing temperature up to ca. 130 °C followed by a rapid decrease with a further increase of temperature up to ca. 140 °C, and then decrease at a very slow rate as the temperature is increased further to 155 °C. Note that the T_{SI} of PABP is ca. 146 °C (Fig. 1). What is unusual in the temperature dependence of G' observed in Fig. 8 for PABP is that values of G' do not decrease steadily when the temperature is increased above its T_{SI}. Such a temperature dependence of G' has never been observed for typical TLCPs without self-association and flexible homopolymers. Therefore, we ascribe the unusual temperature dependence of G' of PABP at elevated temperatures to the presence of self-association within the molecules. Above, referring to Fig. 6 we have pointed out that a weak attractive interaction exists between the pyridyl group in the side-chain azopyridine and hydroxyl groups at the end of the main chain of PABP.

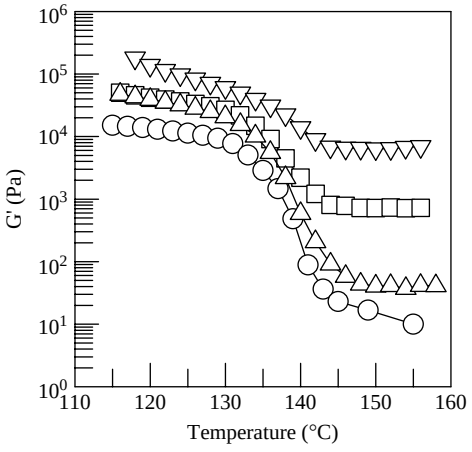

Fig. 8. Variations of G' with temperature during isochronal dynamic temperature sweep experiments at $\omega = 0.1$ rad/s for (○) PABP, (△) PABP/MMT nanocomposite, (□) PABP/Cloisite 20A nanocomposite, and (▽) PABP/Cloisite 30B nanocomposite.

In Fig. 8 we observe further that the temperature dependence of G' for the PABP/MMT nanocomposite is very similar to that of neat PABP, which can be understood from the point of view that little or no attractive interaction exists between PABP and MMT (Fig. 6). However, in Fig. 8 we observe that the temperature dependence of G' for the PABP/Cloisite 20A and PABP/Cloisite 30B nanocomposites is quite different from that for the PABP/MMT nanocomposite. Specifically, values of G' for the PABP/Cloisite 30B nanocomposite at temperatures above the T_{SI} of PABP are exceedingly large (more than two orders of magnitude) compared to those for the PABP/MMT nanocomposite, and about one order of magnitude larger than those for the PABP/Cloisite 20A nanocomposite. In turn, values of G' for the PABP/Cloisite 20A nanocomposite at temperatures above the T_{SI} of PABP are about an order of magnitude larger than those for the PABP/MMT nanocomposite. These observations can be explained from the point of view that strong attractive interactions exist, via hydrogen bonding, between the pyridyl group in the side-chain azopyridine and the hydroxyl group in the surfactant MT2EtOH residing at the surface of organoclay Cloisite 30B. Notice in Fig. 6 that the extent of hydrogen bonding in the PABP/Cloisite 30B nanocomposite is still strong even at temperatures above the T_{SI} (ca. 146 °C) of PABP.

Fig. 9 describes the frequency dependence of the dynamic loss modulus (G'') for (a) PABP, (b) PABP/MMT nanocomposite, (c) PABP/Cloisite 20A nanocomposite, and (d) PABP/Cloisite 30B nanocomposite at various temperatures below and above the T_{SI} of PABP. It is interesting to observe in Fig. 9 that the slope of $\log G''$ versus $\log \omega$ plots in the terminal region is close to one for both neat PABP and PABP/MMT nanocomposite at 160 °C in the isotropic state, usually observed for TLCPs without self-association and flexible homopolymers. However, this observation is at variance with the observation made from the $\log G'$ versus $\log \omega$ plots given in Fig. 7 in that the slope of the $\log G'$ versus $\log \omega$ plots in the terminal region are much less than two, which is not expected from typical TLCPs without self-association in the isotropic state and flexible homopolymers. This difference between the two situations indicates that the elastic property (G') is much more sensitive to the state of self-association of PABP molecules than the viscous property (G'') with G'' being related to dynamic viscosity (η') by $\eta' = G''/\omega$. On the other hand, in Fig. 9(d) we observe clear evidence of the presence of strong attractive interactions in the PABP/Cloisite 30B nanocomposite in that the slope of $\log G''$ versus $\log \omega$ plots

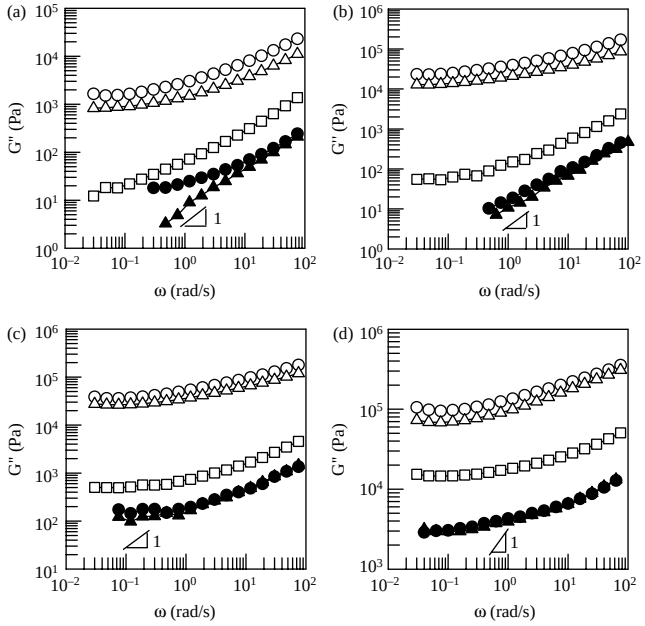

Fig. 9. Log G'' versus log ω plots for (a) PABP, (b) PABP/MMT nanocomposite, (c) PABP/Cloisite 20A nanocomposite, and (d) PABP/Cloisite 30B nanocomposite at different temperatures (°C): (○) 120, (△) 130, (□) 140, (●) 150, and (▲) 160.

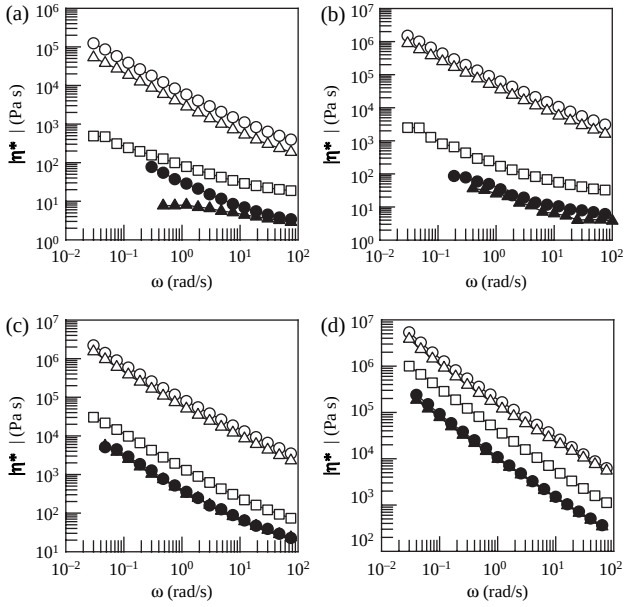

Fig. 10. Log $|\eta^*|$ versus log ω plots for (a) PABP, (b) PABP/MMT nanocomposite, (c) PABP/Cloisite 20A nanocomposite, and (d) PABP/Cloisite 30B nanocomposite at different temperatures (°C): (○) 120, (△) 130, (□) 140, (●) 150, and (▲) 160.

in the terminal region is much less than one in the isotropic state of PABP. Again, in Fig. 9(c) we observe a similar rheological characteristic from the log G'' versus log ω plots in the terminal region for the PABP/Cloisite 20A nanocomposite in the isotropic state. This can be explained by the presence of a very weak interaction in the PABP/Cloisite 20A nanocomposite as evidenced from the FTIR spectrum given in Fig. 6. Notice, however, the difference in the values of G'' between the PABP/Cloisite 30B and PABP/Cloisite 20A nanocomposites in the isotropic state; namely, values of G'' for the PABP/Cloisite 30B nanocomposite are an order of magnitude larger than those for the PABP/Cloisite 20A nanocomposite. As pointed out above, this difference between the two nanocomposites is attributable to the presence of strong attractive interactions in the PABP/Cloisite 30B nanocomposite.

Fig. 10 gives log $|\eta^*|$ versus log ω plots for (a) neat PABP, (b) PABP/MMT nanocomposite, (c) PABP/Cloisite 20A nanocomposite, and (d) PABP/Cloisite 30B nanocomposite at various temperatures below and above the T_{SI} of PABP. The following observations are worth noting in Fig. 10. Referring to Fig. 10(a), neat PABP exhibits a strong frequency dependence of $|\eta^*|$ over the entire range of ω (10^{-2}–10^{2} rad/s) applied at temperatures below the T_{SI} of PABP. It is well established that such a frequency dependence of $|\eta^*|$ is characteristic of TLCP in an anisotropic state, although there is no plateau region (so-called region I) at intermediate angular frequencies. Similar observation has been observed for other TLCPs [47,48]. However, PABP exhibits Newtonian behavior in the terminal region at temperatures well above its T_{SI}. Notice in Fig. 10(a) that log $|\eta^*|$ versus log ω plots for neat PABP at 150 °C, which is only ca. 4 °C above its T_{SI}, still exhibits frequency dependence. This is attributable to the fact that PABP is a polydisperse polymer and thus it cannot have a very sharp, single value of T_{SI}. Therefore, the upper endothermic peak in the DSC thermogram (Fig. 1) should be regarded as an average value of T_{SI} for the polydisperse PABP.

In Fig. 10(b) we observe that the frequency dependence of $|\eta^*|$ for PABP/MMT nanocomposite persists over the entire range of temperatures tested up to 160 °C, which is ca. 14 °C above the T_{SI} of PABP. It should be remembered that values of $|\eta^*|$ come from the contributions of both G' and G'': $|\eta^*(\omega)| = \{[G'(\omega)/\omega]^2 + [G''(\omega)/\omega]^2\}^{1/2}$. Thus, the frequency dependence of $|\eta^*|$ depends on the relative magnitude of G' and G''. Apparently, the contribution of G' is stronger than that of G'' (compare Fig. 7(b) with Fig. 9(b)), giving rise to the frequency dependence of $|\eta^*|$ given in Fig. 10(b).

From the frequency dependence of $|\eta^*|$ given in Fig. 10(c) and (d) we observe that values of $|\eta^*|$ for the PABP/Cloisite 30B nanocomposite are much larger than those for the PABP/Cloisite 20A nanocomposite. This can be explained by the fact that values of both G' and G'' for the PABP/Cloisite 30B nanocomposite are much larger than those for the PABP/Cloisite 20A nanocomposite (compare Fig. 7(c) and (d) with Fig. 9(c) and (d)). Once again, such large values of $|\eta^*|$ for the PABP/Cloisite 30B nanocomposite are attributed to the hydrogen bonding between the pyridyl group in the side-chain azopyridine of PABP and the hydroxyl groups in the surfactant MT2EtOH residing at the surface of Cloisite 30B.

3.4. Rationale for the design and synthesis of PABP for the preparation of organoclay nanocomposites

In the past, a few research groups [35,36] reported on the preparation of organoclay nanocomposites by melt blending based on TLCPs having the following chemical structures,

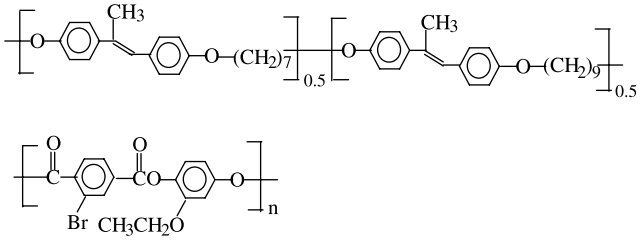

In the preparation of nanocomposites, the authors employed organoclays very similar to Cloisite 30B and Cloisite 20A employed in the present study. They observed large XRD peaks in 2θ scanning [35,36], suggestive of poor dispersion (or intercalation at best) of organoclay aggregates, and indeed intercalated structure as determined by TEM [36]. The above observations were to be expected from the point of view of the absence of specific interaction between the TLCPs and organoclays employed in those studies.

One should keep in mind that in the preparation of organoclay nanocomposites by melt blending, the most important requirement is the presence of specific interactions between the polymer matrix (e.g. TLCP) and organoclay, which can promote compatibility between the two. A close look at the chemical structures of TLCPs shown above and the chemical structure of the surfactant residing at the surface of Cloisite 30B and Cloisite 20A, respectively, reveals that one cannot expect any specific interactions between the TLCPs and organoclays employed [35,36].

On the other hand, the present study has demonstrated unambiguously the presence of specific interactions, via hydrogen bonding, between PABP and Cloisite 30B (Fig. 6), which then gave rise to highly dispersed aggregates of Cloisite 30B (Fig. 5). Most importantly, the liquid crystallinity of PABP in the PABP/Cloisite 30B nanocomposites is more or less intact with a very high degree of dispersion of Cloisite 30B aggregates (Fig. 3(d)). Thus, the rationale for the present study is to demonstrate the fundamental concept for the design and synthesis of TLCP that can give rise to highly dispersed organoclay aggregates in nanocomposites without sacrificing the inherent characteristics (liquid crystallinity) of TLCP. To our knowledge, such a study has never been reported in the literature.

4. Concluding remarks

In this study, we synthesized a segmented main-chain TLCP, PABP, having side-chain azopyridine with flexible spacer to prepare nanocomposites. We have found that PABP is a semicrystalline, smectic-forming TLCP having a T_m of 114 °C and a T_{SI} of 146 °C. In the preparation of nanocomposites we employed natural clay (MMT), an organoclay (Cloisite 20A) treated with a surfactant without polar group, and another organoclay (Cloisite 30B) treated with a surfactant having hydroxyl group. We have found that PABP/Cloisite 30B nanocomposite has a very high degree of dispersion of Cloisite 30B aggregates, while PABP/Cloisite 20A nanocomposite has intercalation of Cloisite 20A aggregates, and PABP/MMT nanocomposite has very poor dispersion of MMT aggregates. Using in situ FTIR spectroscopy we obtained evidence that hydrogen bonds were formed between the pyridyl group in the side-chain azopyridine of PABP and the hydroxyl groups in the surfactant MT2EtOH residing at the surface of Cloisite 30B in the PABP/Cloisite 30B nanocomposite, while very weak interaction in the PABP/Cloisite 20A nanocomposite and no interaction in the PABP/MMT nanocomposite. The present study has demonstrated that successful preparation of organoclay nanocomposites having a very high degree of dispersion of organoclay aggregates depends very much on the extent of compatibility between an organoclay and a thermoplastic polymer. That is, a mismatch or lack of compatibility between an organoclay and a thermoplastic polymer would not produce nanocomposites having a very high degree of dispersion of organoclay aggregates. This has been illustrated in the PABP/Cloisite 20A nanocomposite in that PABP and the surfactant 2M2HT residing at the surface of Cloisite 20A do not have sufficient attractive interactions and thus the nanocomposite gives rise to only intercalation of Cloisite 20A aggregates.

Further, we have found that the mesophase structure (liquid crystallinity) of PABP in the PABP/Cloisite 30B nanocomposite is little affected by the hydrogen bonding between PABP and Cloisite 30B. This is attributed to the fact that the pyridyl group in the side-chain azopyridine of PABP is located sufficiently far away from the mesogenic group of main chain, and thus the hydrogen bonds formed between the pyridyl group at the end of the side-chain azopyridine with five methylene units and the hydroxyl groups in the surfactant MT2EtOH residing at the surface of Cloisite 30B apparently have not interfered with the mobility (thus the orientation) of the mesogenic main chain of PABP. This observation is depicted schematically in Fig. 11, in which the dark ellipsoidal areas represent the mesogens of the main chain interconnected by the flexible spacers (shown by thin waved lines), and the dark sticks represent Cloisite 30B platelets that form hydrogen bonds with the pyridyl group located at the end of side-chain azopyridyl group. Notice in Fig. 11 that the side-chain azopyridyl group is connected to the main chain through five methylene units (shown by thin waved lines). The situation depicted in Fig. 11 is quite different from that depicted in Fig. 11 of Ref. [37], in which the pendent pyridyl group was connected to the mesogenic main chain (PyHQ12, the chemical structure of which is given in the Section 1) only through a vinylene unit and thus the hydrogen bonds formed between the pendent pyridyl group and the hydroxyl groups in the surfactant MT2EtOH residing at the surface of Cloisite 30B might have interfered with the orientation of the mesogenic main chain, consequently disrupting the mesogenic structure of PyHQ12.

In this paper, we have compared the dynamic viscoelastic properties of PABP with those of three nanocomposites prepared. Specifically, we have shown how the dynamic viscoelastic properties of PABP, which has self-association within the molecules, are different from those of typical TLCPs without self-association, and how the hydrogen bonds formed between the pyridyl group in PABP and the surfactant residing

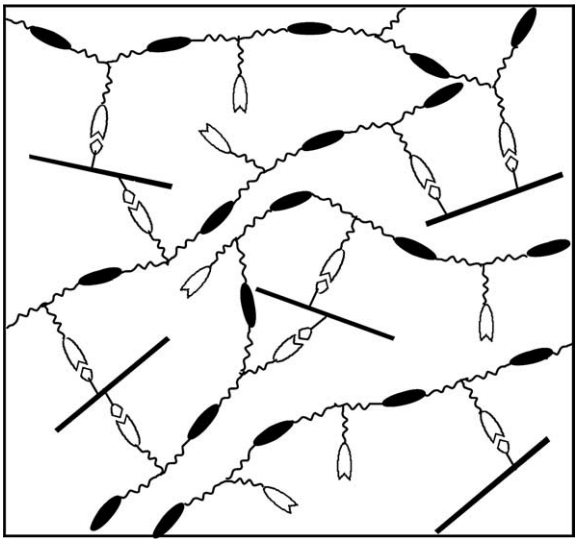

Fig. 11. Schematic describing the distributions of PABP and Cloisite 30B in the highly dispersed PABP/Cloisite 30B nanocomposite, where the dark sticks represent Cloisite 30B platelets, the dark ellipsoids represent the main-chain mesogens, waved lines represent flexible spacers, the empty notched ellipsoids represent the azopyridine in the side chain of PABP, and the empty notched ellipsoids with 'caps' represent hydrogen bonds between the pyridyl group in the side-chain azopyridine of PABP and the hydroxyl groups in the surfactant MT2EtOH residing at the surface of Cloisite 30B.

at the surface of Cloisite 30B affected the dynamic viscoelastic properties of PABP/Cloisite 30B nanocomposite. The present study has demonstrated that rheological measurements, when properly interpreted, can be used as a powerful tool for a better understanding of the dispersion characteristics of organoclay nanocomposites.

Above all, the present study has demonstrated the fundamental concept for the design and synthesis of TLCP that can give rise to a highly dispersed organoclay aggregates in nanocomposites without sacrificing the inherent characteristics (liquid crystallinity) of TLCP. To our knowledge, such a study has never been reported in the literature.

Acknowledgements

This study was supported in part by the National Science Foundation under Grant CST-04006752 and LG Chemical Ltd, for which we are very grateful.

References

[1] About 16,000 references are listed under the title of Nanocomposites in the Science Finder available on the Internet.
[2] Kato M, Usuki A, Okada A. J Appl Polym Sci 1997;66:1781.
[3] Kawasu M, Hasegawa N, Kato M, Usuki A, Okada A. Macromolecules 1997;30:6333.
[4] Hasegawa N, Kawasumi M, Kato M, Usuki A, Okada A. J Appl Polym Sci 1998;67:87.
[5] Liu X, Wu Q. Polymer 2001;42:10013.
[6] Nam PH, Maiti P, Okamoto M, Kotaka T, Hasegawa N, Usuki A. Polymer 2001;42:9633.
[7] Hoffmann B, Kressler J, Stöppelmann G, Fredrich C, Kim GM. Colloid Polym Sci 2000;278:629.
[8] Usuki A, Kawasumi M, Kojima Y, Okada A, Kurauchi T, Kamigaito O. J Mater Res 1993;8:1174.
[9] Usuki A, Kojima Y, Kawasumi M, Okada A, Fukushima Y, Kurauchi T, et al. J Mater Res 1993;8:1179.
[10] Kojima Y, Usuki A, Kawasumi M, Okada A, Kurauchi T, Kamigaito O. J Polym Sci, Polym Chem Ed 1993;31:983.
[11] Yano K, Usuki A, Okada A, Kurauchi T, Kurauchi T, Kamigaito O. J Polym Sci, Polym Chem Ed 1993;31:2493.
[12] Kojima Y, Usuki A, Kawasumi M, Okada A, Kurauchi T, Kamigaito O, et al. J Polym Sci, Polym Phys Ed 1994;32:62.
[13] Sikka M, Cerini LN, Ghosh SS, Winey KI. J Polym Sci, Polym Phys Ed 1996;34:1443.
[14] Hasegawa N, Okamoto H, Kawasumi M, Usuki A. J Appl Polym Sci 1999;74:3359.
[15] Hoffmann B, Dietrich C, Thomann R, Fredrich C, Mülhaupt R. Macromol Rapid Commun 2000;21:57.
[16] Ogata N, Kawakage S, Ohihara T. Polymer 1997;38:5115.
[17] Liu YJ, Schindler JL, DeGroot DC, Kannewurf CR, Hirpo W, Kanatzidis MG. Chem Mater 1996;8:525.
[18] Ogata N, Jimenez G, Kawai H, Ogihara T. J Polym Sci, Polym Phys Ed 1997;35:389.
[19] Fournaris KG, Karakassides MA, Petridis D, Yiannakopoulou K. Chem Mater 1999;11:2372.
[20] Messersmith PB, Giannelis EP. Chem Mater 1993;5:1064.
[21] Messersmith PB, Giannelis EP. J Polym Sci, Polym Phys Ed 1995;33: 1047.
[22] Krishnamoorti R, Giannelis EP. Macromolecules 1997;30:4097.
[23] Jimenez G, Okata N, Kawai H, Ogihara T. J Appl Polym Sci 1997;64: 2211.
[24] Pantoustier N, Alexandre M, Degée P, Calberg C, Jérôme R, Henrist C, et al. e-Polymer 2001;9:1.
[25] Lee KM, Han CD. Polymer 2003;44:4573.
[26] Alexandre M, Beyer G, Henrist C, Cloots R, Rulmont A, Jérôme R, et al. Macromol Rapid Commun 2001;22:643.
[27] Alexandre M, Beyer G, Henrist C, Cloots R, Rulmont A, Jérôme R, et al. Chem Mater 2001;13:3830.
[28] Beyer G. Fire Mater 2001;25:193.
[29] Riva A, Zanetti M, Braglia M, Camino G, Flaqui L. Polym Degrad Stab 2002;77:299.
[30] Lee KM, Han CD. Macromolecules 2003;36:7165.
[31] LeBaron PC, Wang Z, Pinnavaia T. J Appl Clay Sci 1999;15:11.
[32] Kato M, Usuki A. In: Pinnavaia TJ, Beall GW, editors. Polymer–clay nanocomposites. New York: Wiley; 2000. p. 97.
[33] Alexandre M, Dubois P. Mater Sci Eng 2000;28:1.
[34] Ray SS, Okamoto M. Prog Polym Sci 2003;28:1539.
[35] Vaia RA, Giannelis EP. Polymer 2001;42:1281.
[36] Chang JH, Seo BS, Hwang DH. Polymer 2002;43:2969.
[37] Huang W, Han CD. Macromolecules 2006;39:257.
[38] Huang W, Han CD. Macromolecules; in press.
[39] Physical Properties Bulletin from Southern Clay Products, Inc.
[40] Watanabe J. Macromolecules 1988;21:278.
[41] Fischer H, Pose S, Arnold M. Macromolecules 1995;28:6957.
[42] Sato A, Kato T, Uryu T. J Polym Sci, Polym Chem Ed 1996;34:503.
[43] Zhang S, Painter PC, Runt J. Macromolecules 2002;35:8478.
[44] Zhang S, Painter PC, Runt J. Macromolecules 2002;35:9403.
[45] Zhang SH, Jin X, Painter PC, Runt J. Polymer 2004;45:3933.
[46] Coleman MM, Graff JF, Painter PC. Specific interactions and the miscibility of polymer blends. Lancaster: Technomic Publishing; 1991.
[47] Kim SS, Han CD. Polymer 1994;35:93.
[48] Kim DO, Han CD. Macromolecules 2000;33:3349.